THE AMERICAN SOCIETY OF MECHANICAL ENGINEERS
345 E. 47 St., New York, N.Y. 10017







# The Influence of Density Difference Between Hot and Coolant Gas on Film Cooling by a Row of Holes: Predictions and Experiments

**W. HAAS[1], W. RODI, B. SCHÖNUNG[2]**
University of Karlsruhe
Karlsruhe, F.R. Germany

## ABSTRACT

The two-dimensional boundary-layer procedure of Schönung and Rodi [1] for calculating film cooling by a row of holes was extended to account for density differences between hot gas and injected coolant gas. The extensions concern the injection model for leaping over the immediate blowing region in the boundary-layer calculation and also the dispersion model for taking into account three-dimensional effects. The extended model is tested for a density ratio of $\rho_j/\rho_e \approx 2$ both for flat-plate situations and film cooling on a model turbine blade. The predicted laterally averaged film cooling effectiveness is compared with measurements for these cases. Results for the flat-plate experiments were taken from the literature, while experiments for a model turbine blade are also described in this paper. For a fixed injection angle of 32°, the film cooling effectiveness was measured for various spacings and velocity ratios $U_j/U_e$. The density ratio $\rho_j/\rho_e \approx 2$ was achieved by adding Freon to the injection gas. The results are compared with those reported in [2] for negligible density difference. At the same blowing rate $M = U_j/U_e$, the film cooling effectiveness was found to increase with the density ratio $\rho_j/\rho_e$. In general, the influence of the density difference is well predicted by the model.

## NOMENCLATURE

| | |
|---|---|
| D | hole diameter |
| $D_h$, $D_u$, $D_\Theta$ | dispersion terms |
| h | static enthalpy |
| I | momentum, momentum ratio = $(\rho U^2)_j/(\rho U^2)_e$ |
| $\Delta I$ | momentum difference between positions A and B (Fig. 4) |
| k | turbulent kinetic energy |
| M | blowing rate = $(\rho U^2)_j/(\rho U^2)_e$ |
| P | pressure |
| $\Delta P$ | pressure difference between positions A and B (Fig. 4) |
| $Re_l$ | Reynolds numbers based on chord ength and inlet conditions |
| s | hole spacing |
| T | temperature |
| Tu | free-stream turbulence level in percent |
| U | velocity component in x-direction |
| $y_{max}$, $y_{wen}$ | parameters in injection model for dimensionless temperature |
| $y_{imin}$, $y_{imax}$, $y_{iend}$ | parameters in injection model for momentum |
| x,y,z | Cartesian coordinates |
| $\alpha$ | injection angle |
| $\delta$ | boundary-layer thickness |
| $\delta^*$ | boundary-layer displacement thickness $= \int_0^\infty (1 - \rho U/\rho_e U_e) dy$ |
| $\varepsilon$ | dissipation rate |
| $\bar{\eta}$ | laterally averaged cooling effectiveness |
| $\Theta$ | dimensionless temperature, tracer concentration $= (T - T_e)/(T_j - T_e)$ |
| $\rho$ | fluid density |

Subscripts

| | |
|---|---|
| a | adiabatic wall |
| A | value before injection region (Fig. 4) |
| B | value after injection region (Fig. 4) |
| e | free-stream (external) value |
| j | injection value |
| max | maximum |
| min | minimum |
| wall | value on the wall |

[1] present address: Betriebsforschungsinstitut, Düsseldorf, F.R. Germany
[2] present address: ABB Turbosystems, Baden, Switzerland

Presented at the International Gas Turbine and Aeroengine Congress and Exposition
Orlando, FL June 3-6, 1991
This paper has been accepted for publication in the Transactions of the ASME
Discussion of it will be accepted at ASME Headquarters until September 30, 1991

## 1. INTRODUCTION

The desire for higher thermal efficiency of gas turbines has led to higher and higher temperatures at the inlet of the turbine section. The temperatures have reached such high levels that the turbine blades need to be protected by efficient cooling. One of the most efficient cooling methods is film cooling by injection of cooling fluid through rows of holes, and this method is now widely used in practice. Already for one row of holes, for which the flow situation is shown in Fig. 1, a very complex flow develops with a wide variety of influence parameters such as the blowing angle $\alpha$, the relative spacing s/D, the velocity ratio $U_j/U_e$, the density ratio $\rho_j/\rho_e$ and the state of the oncoming boundary layer. The cooling air tapped from the compressor causes a flow loss, and there are further losses associated with the injection itself. Under unfavourable conditions, the gain achieved by the film cooling can be used up by the flow losses, and hence the amount of cooling air must be kept at a minimum. This requires a delicate optimisation of the film cooling design. As there are many influence parameters involved, optimisation with the aid of experiments is not really feasible and a reliable prediction method is needed.

The flow field in the vicinity of injection holes is strongly three-dimensional and it is also associated with reverse flow which is governed by elliptic equations rather than by parabolic boundary-layer equations. Hence, basically a

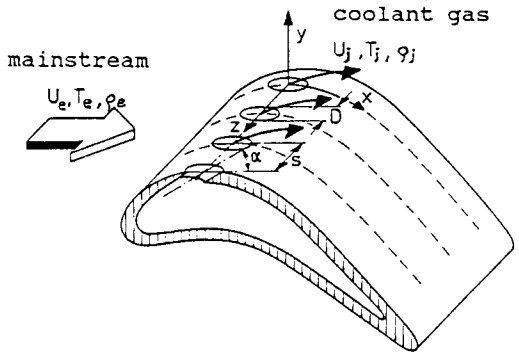


Fig. 1: Flow configuration

three-dimensional elliptic calculation procedure is necessary for simulating the film cooling flow. Such methods are now available, but as the review of Schönung and Rodi [1] has shown, these methods are still too costly for carrying out parameter studies necessary for optimising the film cooling design. Hence, much faster two-dimensional boundary-layer methods are highly desirable. Schönung and Rodi [1] have developed such a method, in which the elliptic reverse-flow region in the vicinity of the injection holes is leapt over and new boundary-layer profiles are set up downstream of this region with an injection model, while the three-dimensional effects are simulated with the aid of dispersion terms appearing in the 2D boundary-layer equations. Both the injection and the dispersion model were developed with the aid of systematic 3D film cooling calculations covering a wide range of injection angles $\alpha$, velocity ratios $U_j/U_e$ and relative spacings s/D. The 2D boundary-layer method of Schönung and Rodi [1] covers the full range of these parameters of practical interest, and test calculations carried out for a wide variety of these parameters showed fairly good agreement with experiments in most cases. However, although the density is formaly included as a variable in this model, the influence of density ratio of hot and coolant gas cannot be simulated realistically because the injection and dispersion models were based on 3D calculations for a density ratio of 1. In this paper, therefore, the film cooling model of Schönung and Rodi is extended to include the effects of density ratio $\rho_j/\rho_e$. For verification purposes, experiments were carried out on a model turbine blade for a density ratio of $\rho_j/\rho_e = 2$ as an extension of the experiments with $\rho_j/\rho_e = 1$ reported in detail by Haas et al. [2]. These experiments are also reported in this paper, and the calculations are compared with these experiments as well as with experiments for flat-plate situations taken from the literature.

## 2. FILM COOLING MODEL

### 2.1 Basic Flow Features

For the development of a film cooling model it is important to know the basic flow phenomena occurring in the vicinity of injection holes. Hence, a brief description of these phenomena is given by considering the injection of a single jet as sketched in Fig. 2. Two regions of the flow with 3D behaviour can be distinguished. In the immediate vicinity of the injection hole, pressure forces are important which cause a bending-over of the injected jet due to the high upstream pressure and in certain cases also reverse flow behind the jet due to the low pressure in this region.

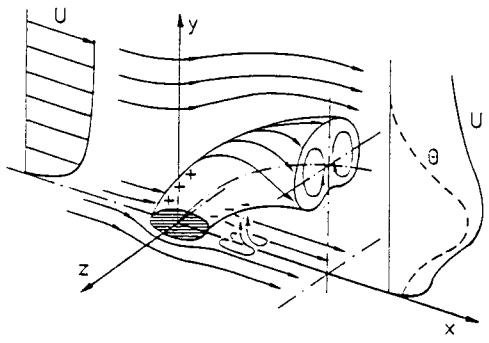


Fig. 2: Flow field in the vicinity of a single jet in a cross flow

Owing to the shearing of the bending-over jet by the cross flow, longitudinal vorticity is generated which leads to the secondary motion sketched in Fig. 2 and consequently to the kidney shape of the bent-over jet. Simultaneously with the bending-over, mixing between the jet fluid and the oncoming fluid occurs, thereby reducing the excess or deficit velocity of the jet. The penetration of the jet depends mainly on the injection angle $\alpha$ and on the momentum ratio $I = (\rho U^2)_j/(\rho U^2)_e$ and can lead to strongly different characteristics behind the injection. For large $\alpha$ and I, the flow is of wake character and is similar to the flow past a solid cylinder placed on the wall. Downstream of the bent-over jet a reverse-flow zone develops into which hot gas is mixed in from the side. Past the reverse-

flow zone the jet attaches on the blade surface. At small momentum ratios I, the jet bends over very quickly and attaches to the wall. When the injection angle is small, the jet also attaches quickly to the wall and at higher momentum ratios the flow develops wall-jet character.

When the bending-over of the jet is complete and the jet has attached to the wall, pressure forces are small and the flow development is mainly determined by turbulent mixing. The flow has regained its boundary-layer character, but it is still three-dimensional and, as sketched in Fig. 2, the velocity and temperature profiles differ strongly from those in developed boundary layers. In this region, the individual jets grow together so that after some distance the spanwise variations disappear and the flow becomes two-dimensional. This process depends not only on the injection angle and the momentum ratio but also on the relative spacing. For large spacing and when the jets penetrate into the cross flow, the individual jets merge only at larger downstream distances.

The dependence of the phenomena described above on the various flow parameters must be described realistically by the film cooling model. In the present study, the injection angle $\alpha$, the relative spacing s/D, the velocity ratio $U_j/U_e$ and the density ratio $\rho_j/\rho_e$ (defining together the momentum ratio I) are in the foreground. Additional parameters that influence the film cooling characteristics are the state of the oncoming boundary layer (laminar or turbulent), the ratio of boundary layer thickness to injection hole diameter, the surface curvature, the longitudinal pressure gradient and the free-stream turbulence level.

## 2.2 Basic Calculation Procedure

The 2D boundary layer calculation procedure of Schönung and Rodi [1] formed the basis of the present work. The boundary layer equations, the low-Reynolds-number k-ε model used for simulating the turbulent momentum and heat transfer and the marching-forward finite-volume method for solving the flow equations are described in [1]. The complex flow phenomena sketched in Section 2.1 can be simulated with a 2D boundary layer procedure only when special measures are taken. This is is done in the film cooling model of Schönung and Rodi [1] by introducing an injection model and a dispersion model which will now be summarised briefly.

Injection model. The region near the injection is leapt over and new boundary layer profiles are set up at a certain distance behind the blowing region. These profiles take into account the characteristics of the oncoming boundary layer as well as of the injected jets.

Dispersion model. Formal lateral averaging of the three-dimensional equations leads to two-dimensional equations with additional terms accounting for the lateral variation of the flow quantities and the additional lateral mixing. These so-called dispersion terms are modelled as additional source and sink terms in the 2D boundary layer equations and cause a redistribution of the laterally averaged quantities in the y-direction normal to the wall.

Both models are based on the results of 3D elliptic calculations which Demuren et al. [3] have carried out for 27 different film cooling configurations for the flat-plate situation. A detailed analysis of these results provided the necessary information for setting up the boundary layer profiles of the injection model and for the distribution of the dispersion terms in the dispersion model. The injection model contains 10 parameters which are used for generating boundary-layer profiles past the injection and the dispersion model contains 5 parameters with which the three-dimensional effects are described. The values of these parameters are stored in the calculation procedure in form of a coefficient matrix for 100 film cooling configurations depending on the injection angle $\alpha$, the relative spacing s/D and the velocity ratio $U_j/U_e$. By interpolation of the stored coefficient matrix, film cooling configurations can be calculated in the following ranges of the influence parameters:

$$\begin{array}{lcll} 0^o & < & \alpha & \leq & 90^o \\ 1.2 & \leq & s/D & \leq & 10.0 \\ 0 & \leq & U_j/U_e & & 4.0 \end{array}$$

As the 3D calculations of Demuren et al. [3] were all for a density ratio $\rho_j/\rho_e = 1$, they provided no information on density effects, and the model was in fact found to produce unrealistic results when the density ratio was significantly different from 1. Hence, in the following section the injection and dispersion models are extended to account for the influence of significant density differences between hot and coolant gas.

## 2.3 Model Extension to Account for the Effect of Density Differences

The extension of the film cooling model was carried out step by step, starting with a revision of the correlations stored in the calculation procedure for generating the restart boundary-layer and the dispersion profiles. To this end, the parameters in the film cooling model were written in dimensionless form so that the influence parameters characterising the film cooling configuration can be accounted for directly. This also simplified the physical interpretation of the basic mechanisms. The effect of the density ratio $\rho_j/\rho_e$ was brought into the model with the aid of similarity considerations and with experimental information available from the literature. This revealed that the blowing rate $M = (\rho U)_j/(\rho U)_e$, which is often used in film cooling studies, is not so suitable for the film cooling model developed here. The blowing rate M is a measure of the mass flux injected into the boundary layer, but the dynamics of the flow field are better characterised by the momentum ratio

$$I = \frac{(\rho U^2)_j}{(\rho U^2)_e} \qquad (1)$$

This ratio determines the penetration of the cooling jets into the hot-gas stream and is therefore relevant for the distribution of the injected cooling air in the near-field of the injection holes. Hence, the momentum ratio I is used in the extended model as an additional parameter for generating the restart boundary-layer profiles. Further, by combining various parameters and by expressing some of the correlations in analytical form, the number of parameters stored in the calculation procedure could be reduced from 15 to 10. In the following, the extension of the film cooling model to account for the effect of density differences is briefly sketched; details of the model extension can be found in [4, 5].

2.3.1 Injection Model

The location B (see Fig. 3) at which the restart boundary-layer profiles are prescribed after the injection has been correlated with the aid of the 3D results as described in [1]. The velocity profile at this location is determined with the aid of the one-dimensional momentum balance

$$\Delta I(y) = \underbrace{\rho_B(y)U_B^2(y)}_{I_B(y)} - \underbrace{\rho_A(y)U_A^2(y)}_{I_A(y)} = I_j(y) - \Delta P(y) \quad (2)$$

for layers sketched in Fig. 3. In (2), $I_B(y)$ is the momentum distribution at location B downstream of the injection and $I_A(y)$ is the momentum distribution in the oncoming boundary layer which follows from a normal boundary layer calculation upstream of the injection. The distribution of the injected momentum is described by $I_j(y)$ while $\Delta P(y)$ accounts for the pressure difference between locations A before and B after the injection. It should be noted that the pressure is not yet uniform at location B where the boundary layer profiles are set up.

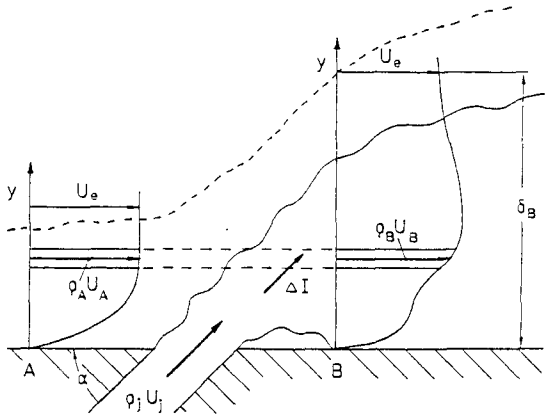


Fig. 3: Control-volume layer for one-dimensional momentum balance

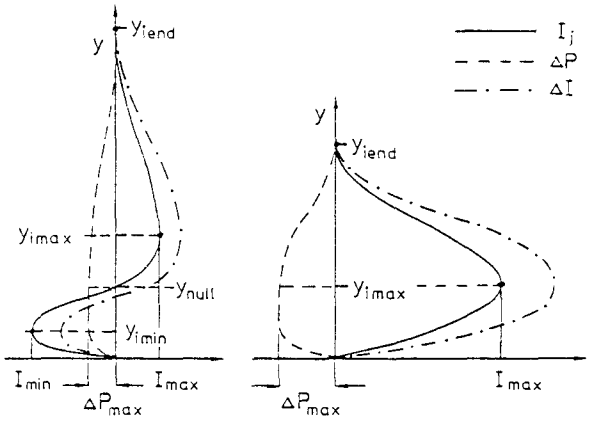


a) Flow with wake character b) Flow with wall-jet character

Fig. 4: Modelling of the momentum distribution

Fig. 4 shows two typical profiles of the injected momentum $I_j$, the pressure difference $\Delta P$ and the difference $\Delta I$ between inflowing and outflowing momentum. The profiles in Fig. 4a correspond to a wake-flow situation as it occurs in most film cooling situations, so for $\alpha < 30^o$ with small and medium velocity ratios $U_j/U_e$ and for $\alpha > 60^o$ when the velocity ratio is high. Only when $\alpha$ is small and $U_j/U_e > 1$ is the flow downstream of the injection of wall-jet character, and the distributions in Fig. 4b are for this situation. As in the basic model, the excess momentum $I_{max}$ is determined such that integration over the modelled injection momentum distribution $I_j(y)$ yields the total momentum discharged by the jet. The parameters $y_{imin}$, $y_{imax}$ and $y_{iend}$ defining the distribution $I_j$ (y) are correlated with the injection angle $\alpha$ and the momentum ratio I but are virtually independent of the relative spacing s/D. The model relations for the other parameters were simplified somewhat over those in the basic model .

For determining the re-start temperature distribution at location B, the laterally averaged adiabatic temperature

$$\Theta_B(y) = \frac{T_a(y) - T_e}{T_j - T_e} \quad (3)$$

is used. This corresponds to the temperature under adiabatic conditions and can be the considered as a tracer-concentration distribution with which the spreading of the cooling jets can be characterised. The realistic approximation of this distribution was very important for extending the film cooling model to situations with strong density differences. A typical profile of the adiabatic temperature is shown in the left part of Fig. 5. The parameters stored in the calculation procedure for generating this distribution are $y_{max}$, $y_{wen}$ and $\Theta_{wall}$. The parameter $y_{max}/D$ was correlated with $U_j/U_e$ and the difference $(y_{wen} - y_{max})/D$ with the momentum ratio I. This modelling causes a widening of the tracer-concentration distribution normal to the wall when the density ratio $\rho_j/\rho_e$ increases, thereby accounting for the larger input of mass and enthalpy. Immediately downstream of the injection, the adiabatic wall temperature $\Theta_{wall}$ correlates with the velocity ratio $U_j/U_e$ and is independent of the density ratio $\rho_j/\rho_e$, as became obvious from the evaluation of measurements for different film cooling configurations [6 - 8]. However, this statement is valid only for sufficiently large momentum ratios. Below a limiting value of $I \approx 0.1$, the adiabatic wall temperature correlates with the momentum ratio I [8, 9].

Another important aspect of the model extension is the use of balance equations for tracer mass and enthalpy. The maximum value of the tracer distribution shown in Fig. 5, $\Theta_{max}$, is calculated iteratively from the following balance equation:

$$\int_0^{y_e} (\rho U \Theta)_B dy = \frac{\pi D^2}{4s} \rho_j U_j \quad (4)$$

where the left-hand side is the tracer mass flux at location B and the right-hand side is the injected mass (note that the injected tracer concentration is 1 according to (3)). An estimated value of $\Theta_{max}$ needed for the first iteration is obtained from a correlation provided by the basic film cooling model.

The parameters for generating the tracer distribution are

now known, and with this the temperature distribution $T_B(y)$ and also the density distribution $\rho_B(y)$ at location B downstream of the injection can now be determined. The corresponding velocity profile $U_B(y)$ is calculated iteratively with the aid of equation (2). For non-adiabatic walls, the temperature distribution $T_B(y)$ to be set up is not identical with the distribution of the adiabatic temperature since the temperature distribution in the oncoming boundary layer has to be accounted for. This is achieved with the following relation:

$$T_B(y) = T_e + \Theta_B(y)(T_j - T_e) + \sigma\left[T_A(y) - T_e\right] \qquad (5)$$

Here, $T_A(y)$ is the temperature profile at location A upstream of the injection, which follows from a normal boundary layer calculation. The parameter $\sigma = (1 - D/s)$ takes account of the part of the oncoming boundary layer which extends to the region between the cooling jets in the vicinity of the injection holes.

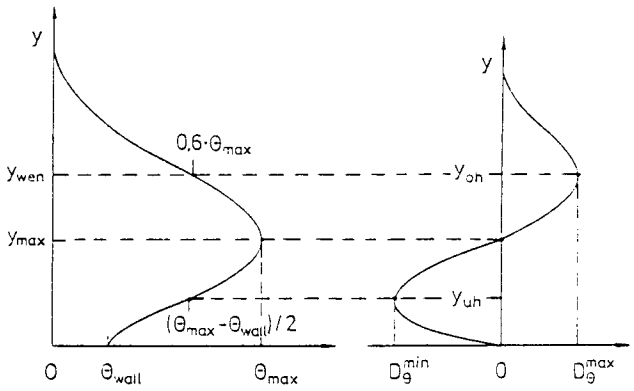


Fig. 5: Distributions of laterally averaged adiabatic temperature $\Theta_B(y)$and dispersion term $D_\theta$ past the injection

For generating the enthalpy distribution at location B, a balance equation analagous to (4) is used:

$$\int_0^{y_e} \left[(\rho U h)_B - (\rho U h)_A\right] dy = \frac{\pi D^2}{4s} \rho_j U_j (h_j - h_e) \qquad (6)$$

Here, $h_j - h_e$ is the difference in static enthalpy between the oncoming flow and the coolant. The profile of the static enthalpy $h_B(y)$ at location B is calculated from the temperature distribution $T_B(y)$ in the iterative process.

For setting up the restart profiles of turbulence quantities at location B, the distribution of turbulent energy in the cooling jets is superimposed to the energy distribution in the oncoming boundary layer. The boundary-layer measurements reported in [5] have shown that the distribution of the turbulent energy due to the cooling jets can be described by a profile similar to that for the adiabatic temperature $\Theta_B(y)$. A maximum of this distribution is obtained with the aid of a correlation derived from measurements [5]. The dissipation rate $\varepsilon$ is determined with the aid of a mixing-length model, in which the turbulent length scale of the oncoming boundary layer and of the injection jets is accounted for.

### 2.3.2 Dispersion model

Dispersion terms representing 3D effects are introduced into the 2D equations for the velocity U, the adiabatic temperature $\Theta$ and the enthalpy h. Dispersion terms for the turbulence quantities k and $\varepsilon$ are considered negligible compared with the source and sink terms in the k- and $\varepsilon$-equations. A typical distribution of a dispersion term $D_\Theta$ for the adiabatic temperature $\Theta$ as determined from the 3D calculations is shown on the right-hand side of Fig. 5 for a position just downstream of the injection. The principles of the dispersion model are now explained with the aid of this distribution. $D_\Theta$ is negative near the wall and positive in the outer part of the boundary layer, describing the lifting of the coolant jets by the lateral entrainment of hot gas near the wall. As can be seen from Fig. 5, the position of the maximum $D_\Theta^{max}$ and the minimum $D_\Theta^{min}$ and the zero crossing are closely related to the distribution of the adiabatic temperature $\Theta$. The value of the near-wall minimum, $D_\Theta^{min}$, is calculated with the aid of coefficients stored in the calculation procedure, and the decay of the dispersion terms with streamwise distance from the injection is described with the aid of exponential functions. The maximum value $D_\Theta^{max}$ in the outer part of the boundary layer is calculated from the constraint that the integral over the dispersion distribution has to be zero since dispersion terms do not produce any net sources and sinks but only a redistribution of the quantity in question. For reasons of momentum conservation, the pressure difference introduced according to equation (2) must be removed further downstream, and this is described by an additional source term in the dispersion model. As dispersion terms physically represent fluxes, the density effect is accounted for simply by multiplying the dispersion terms obtained without density variation with the local density ratio $\rho(y)/\rho_e$. The dispersion term for the enthalpy h calculated from the $\Theta$-dispersion term is as follows:

$$D_h(y) = D_\Theta(y)\left[h_j - h_e - \sigma\ (h_A(y) - h_e)\right] \qquad (7)$$

The term $h_A(y) - h_e$ represents the profile of the static enthalpy upstream of the injection. This term is multiplied with the factor $\sigma = (1\text{-}s/D)$ in order to account in a similar way to equation (5) for the influence of the oncoming boundary layer which penetrates between the coolant jets into a limited region downstream of the injection.

## 3. MEASUREMENTS OF FILM COOLING EFFECTIVENESS ON A MODEL TURBINE BLADE

In order to allow a realistic testing of the film cooling model, film cooling experiments were carried out on a model blade. These are an extension of the measurements described in [2] for a density ratio of $\rho_j/\rho_e \approx 1$. The experimental apparatus, the measurement blade and the measurement techniques are described in detail in [2] and are only briefly sketched here. The measurements were carried out on an enlarged model of a relatively thin, highly curved turbine blade (see Fig. 6). The "cooling" gas was injected on the suction side through a row of holes at a relative surface distance of 25% and at an injection angle of $\alpha = 32^o$. The hole diameter D was chosen such that the ratio $\delta/D$ assumes a value of about 0.3 typical for real turbine blades. In the measurements presented here, the relative spacing s/D and the blowing rate M were varied.

The Reynolds number based on the chord length (0.25 m) and the oncoming velocity was $Re_1 \approx 1.4 \times 10^5$, and the turbulence level of the free-stream was $Tu_1 = 6.2\%$. The injected air was heated, and the laterally averaged film cooling effectiveness $\bar{\eta}$ was determined by measuring the adiabatic wall temperature. In real film cooling situations, the density ratio is $\rho_j/\rho_e \approx 2$, and this density ratio was achieved by adding Freon to the injected air. Measurements for the density ratio of $\rho_j/\rho_e \approx 1$ (without addition of Freon) were reported already in [2]. Because of heat transfer from the duct supplying the heated injection air placed in the front part of the blade (see Fig. 6), the conditions at the blade surface upstream of the injection were not adiabatic. A temperature boundary layer developed in this region, which had to be taken into account in the calculations. The measured distributions of the film cooling effectiveness are presented together with the calculation results in Section 4.2.

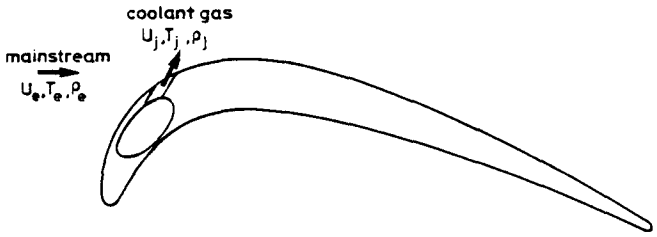


Fig. 6: Model turbine blade

## 4. COMPARISON OF PREDICTIONS WITH MEASUREMENTS

The extended film cooling model was tested first extensively for film cooling situations with small density differences. The results reported in [4, 5] demonstrate that, in general, the extended model leads to better agreement with measurements than the basic version. The present paper presents predictions for cases with density ratios occurring in practice, i.e. for $\rho_j/\rho_e \approx 2$. The model is tested first against measurements available in the literature for plat-plate situations and then against the own measurements on a model turbine blade described in Section 3. It should be mentioned here that the numerical uncertainty of the calculation procedure is very small; it is certainly negligible compared with the uncertainties introduced by the injection and dispersion models.

### 4.1 Film Cooling Effectiveness on Flat Plates

In the flat-plate experiments simulated, the density difference was achieved by injecting a Freon-air mixture and the film cooling effectiveness $\eta$ was obtained from wall concentration measurements. Since the equations governing heat and mass transfer are the same, the density difference could be simulated in the calculations by the temperature difference.

The first set of experiments simulated were those due to Pedersen et al. [9] who investigated film cooling for an injection angle $\alpha$ of $\alpha = 35^o$ and a spacing of $s/D = 3$. The free-stream velocity was $U_e = 15.4$ m/s and the free-stream

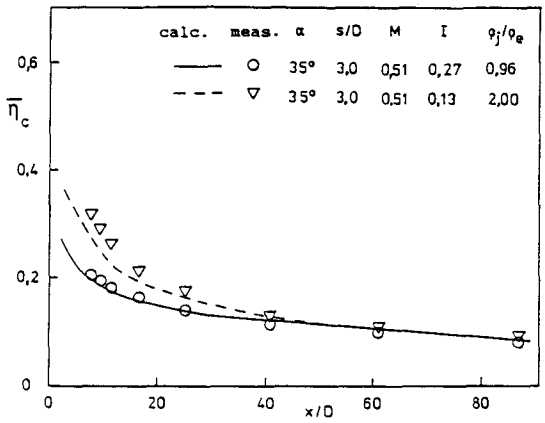


Fig. 7: Cooling effectiveness on flat plate at $M \approx 0.5$ and different density ratios; measurements of Pedersen et al. [9]

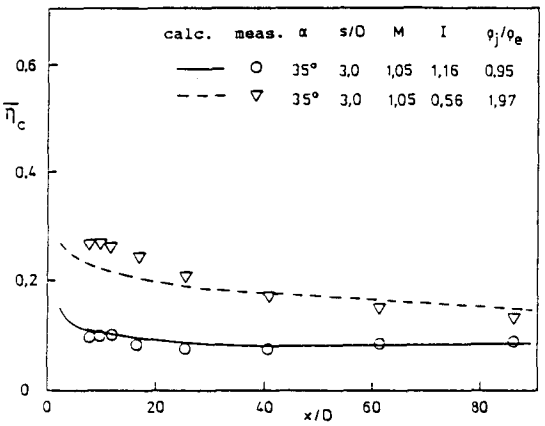


Fig. 8: Cooling effectiveness on flat plate at $M \approx 1$ and different density ratios; measurements of Pedersen et al. [9]

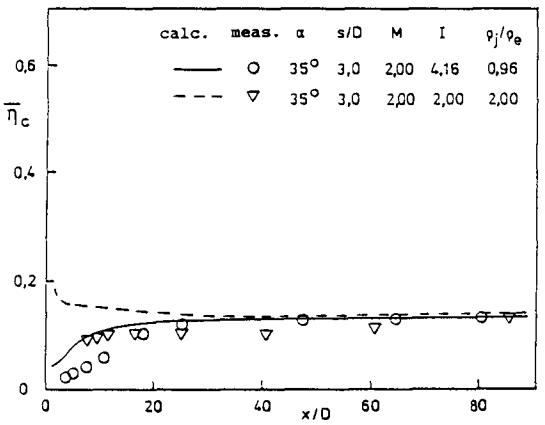


Fig. 9: Cooling effectiveness on flat plate at $M \approx 2$ and different density ratios; measurements of Pedersen et al. [9]

turbulence level $Tu_e$ = 0.4%. The oncoming boundary layer was turbulent and its relative displacement thickness was $\delta^*/D$ = 0.16. For various blowing rates, each of the following figures includes results for density ratios 1 and 2. While for $\rho_j/\rho_e = 1$, the velocity ratio $U_j/U_e$ is identical with the blowing rate, the velocity and momentum ratio is only half for $\rho_j/\rho_e = 2$.

Fig. 7 compares calculated and measured streamwise distributions of the laterally averaged film cooling effectiveness for M = 0.5. In the vicinity of the injection down to x/D = 40, the measured $\overline{\eta}$ -values are higher for the larger density ratio, which is due to the faster reattachment of the cooling air jets at the smaller momentum ratio. In the far-field, the film cooling effectiveness does not depend on the density ratio because the mixing is more or less complete so that the density difference has disappeared. The increase in cooling effectiveness by increasing the density ratio is much stronger in the case of M ≈ 1 (Fig. 8). While the $\overline{\eta}$-distribution for $\rho_j/\rho_e \approx 1$ indicates a penetration of the cooling jets into the free-stream, the variation and the higher values of $\overline{\eta}$ for $\rho_j/\rho_e \approx 2$ point to a wall-jet character of the flow. These differences in the flow character can also explain the large differences in $\overline{\eta}$ far downstream. This result is consistent with the general experimental observation that for similar spacings the best cooling effectiveness is always achieved at $U_j/U_e \approx 0.5$. At a blowing rate of M = 2 (Fig. 9) the measurements clearly indicate a detachment of the cooling jet from the wall. Since there is no difference in $\overline{\eta}$ in the far field, it may be concluded that the jet character is not influenced significantly by the density difference.

Except for fairly small deviations near the injection, the calculation procedure describes realistically the influence of the density ratio on the cooling effectiveness. In view of the complexity of the flow in the near-field and of the simplicity of the model, the discrepancies in this region are not surprising. The good performance in the far-field justifies the assumptions made in the model.

As further test cases, the experiments of Foster and Lampard [10] were simulated. The relative spacing was s/D = 3 and the injection hole diameter D = 2.27 mm. These experimentors investigated the cooling effectiveness for injection angles of $\alpha$ = 35°, 55° and 90° at blowing rates of M = 0.5 and M = 1.4. The free-stream velocity was 25 m/s. Foster and Lampard [10] do not report the free-stream turbulence level. Judging from their experimental set-up a value of $Tu_e$ = 1% was assumed for the calculations. The oncoming boundary layer was also turbulent and had a relative displacement thickness of $\delta^*/D$ = 0.16. For these experiments, different figures show results for different injection angles for both M = 0.5 and M = 1.4. Fig. 10 displays the distribution of the film cooling effectiveness for $\alpha$ = 35°. Both measurements and calculations show similiar behaviour as for the test cases of Pedersen et al. [9]. Fig. 11 reports the results for $\alpha$ = 55°. Due to the larger injection angle, the cooling effectiveness for M = 0.5 is reduced near the injection holes, while for M = 1.4 it increases. In the far-field, the measurements approach the same level as in the case with $\alpha$ = 35°. For M = 0.5, the calculation reproduces this behaviour correctly, but for M = 1.4 it underpredicts the cooling effectiveness. The trend observed for $\alpha$ = 55° continues when the injection angle is increased to $\alpha$ = 90° and is reproduced correctly by the

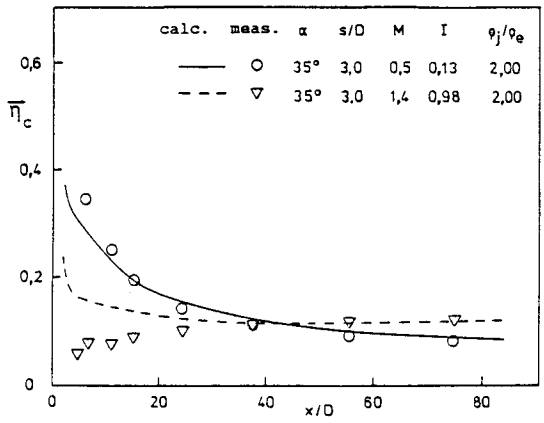


Fig. 10: Cooling effectiveness on flat plate at $\alpha$ = 35°, $\rho_j/\rho_e$ = 2.0 and different blowing rates; measurements of Foster and Lampard [10]

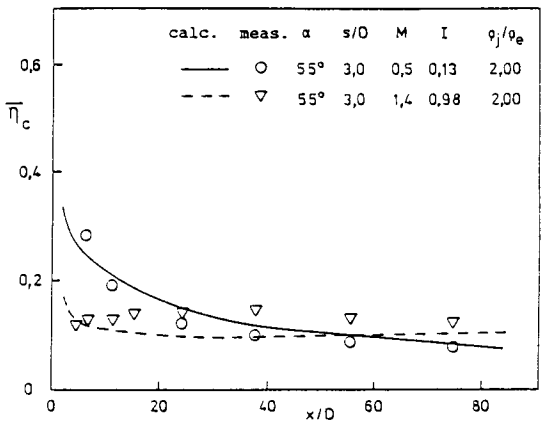


Fig. 11: Cooling effectiveness on flat plate at $\alpha$ = 55°, $\rho_j/\rho_e$ = 2.0 and different blowing rates; measurements of Foster and Lampard [10]

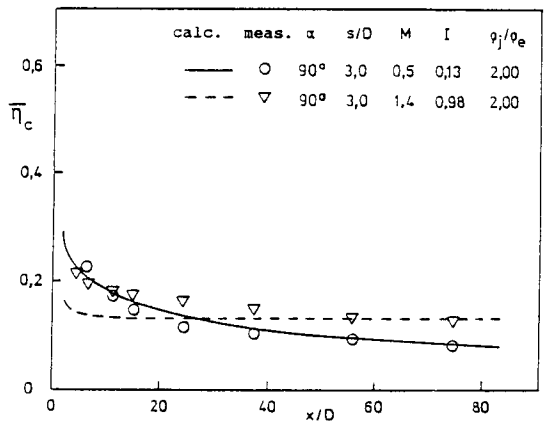


Fig. 12: Cooling effectiveness on flat plate at $\alpha$ = 90°, $\rho_j/\rho_e$ = 2.0 and different blowing rates; measurements of Foster and Lampard [10]

calculations (see Fig. 12). The increase in cooling effectiveness with increasing injection angle for M = 1.4 deserves special attention. It appears that this behaviour is caused by the faster lateral mixing of the injected jets, an effect which is simulated correctly by the calculation procedure. This points to good reliability of the dispersion model also for larger density differences.

## 4.2 Film Cooling Effectiveness on a Model Turbine Blade

In this section, film cooling on a model turbine blade (Fig. 6) investigated in the experiments of Section 3 was simulated. As was mentioned already, the development of a temperature boundary layer upstream of the injection had to be taken into account. To this end, the heat fluxes in the leading edge region of the blade were determined first by a separate boundary layer calculation, and these fluxes were then prescribed as boundary condition upstream of the injection in the calculation of the film cooling effectiveness. In contrast to the flat plate test cases, the oncoming boundary layer was laminar on the model turbine blade ($\delta^*/D = 0.06$). It was assumed that the injection would cause transition and hence turbulent injection profiles were set up as in the other cases.

The test cases for which results are presented in Figs. 13 to 16 show that, at the same blowing rate, the cooling effectiveness $\bar{\eta}$ is considerably higher for the larger density ratio $\rho_j/\rho_e \approx 2$ than for $\rho_j/\rho_e \approx 1$. This was to be expected and corresponds to the results for the flat-plate situations discussed in the previous section. This influence can be explained by the smaller momentum of the coolant jets at larger density ratio but at the same M. The smaller injection momentum causes a faster bending-over of the jets, which in turn leads to a higher cooling effectiveness. For s/D = 3 and M ≈ 1 (Fig. 13), the calculated $\bar{\eta}$ for $\rho_j/\rho_e \approx 1$ is somewhat lower than the measurements. This is presumably due to surface curvature effects, which are not accounted for in the calculation procedure. As shown in the work of Ito et al. [11], convex wall curvature causes a faster attachment of the jet (higher cooling effectiveness) at small blowing rates while it causes a deeper penetration of the jet into the free-stream (lower effectiveness) at large blowing rates. For $\rho_j/\rho_e \approx 2$ the cooling effectiveness is underpredicted somewhat in the initial region, but the overall distribution is well simulated. In the case s/D = 3 and M ≈ 1.4 (Fig. 14), the calculations are in good accord with the measurements.

Figs. 15 and 16 show the corresponding $\bar{\eta}$-distributions for s/D = 4.5. The influence of the density ratio is similar to that for the spacing s/D = 3. The discrepancies between predictions and measurements are again stronger for M = 1 than for M = 1.5. This is consistent with the findings of Ito et al. [11] who correlate the influence of the wall curvature on film cooling with the parameter $I\cos^2\alpha$ . For higher momentum ratios I the curvature effect causes a deeper penetration of the jets into the free-stream while for lower momentum ratios a faster attachment of the jets on the wall results. Hence the calculation, which does not account for any curvature effects, generally underpredicts the $\bar{\eta}$-values for large momentum ratios.

Fig. 17 compares calculated and measured $\bar{\eta}$-distributions for the small spacing s/D = 1.5 and for the small blowing rate M = 0.5 (further measurements could not be carried out for this spacing). In this case, the cooling effectiveness

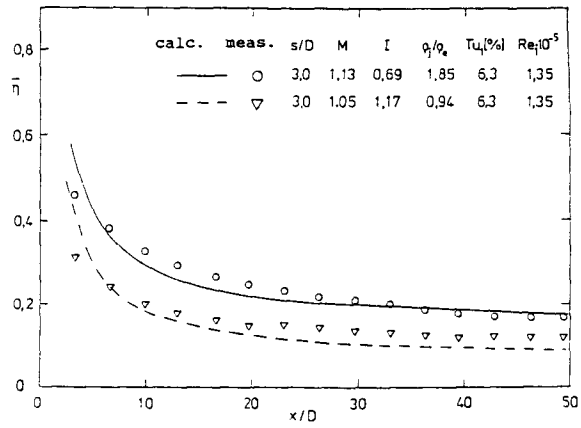


Fig. 13: Cooling effectiveness on model turbine blade at s/D = 3.0, M ≈ 1 and different density ratios; own measurements

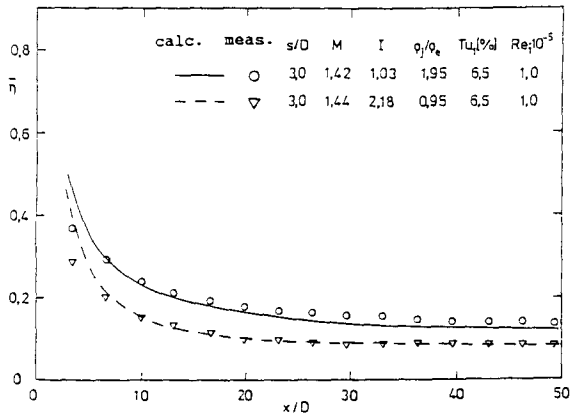


Fig. 14: Cooling effectiveness on model turbine blade at s/D = 3.0, M ≈ 1.4 and different density ratios; own measurements

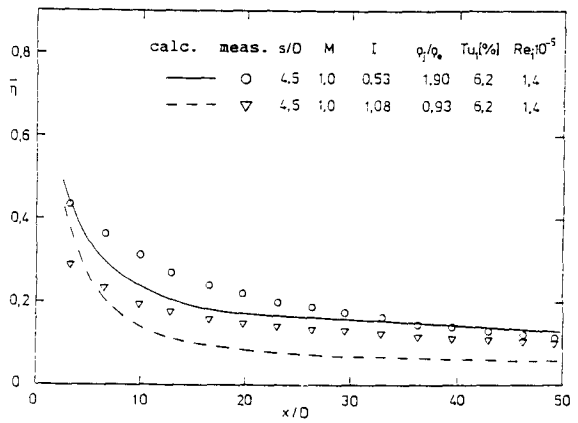


Fig. 15: Cooling effectiveness on model turbine blade at s/D = 4.5, M = 1.0 and different density ratios; own measurements

is larger for $\rho_j/\rho_e$ = 1.9 than for $\rho_j/\rho_e$ = 0.9 only directly behind the injection, while downstream of x/D = 7 the situation is reversed and hence different from that discussed in Figs. 13 to 16. In the initial region, the faster bending-over of the jets again causes an increase in $\bar{\eta}$. Subsequently, a laterally coherent wall jet with a velocity deficit is formed at the small M and s/D values. The velocity deficit is larger for the larger injection density causing larger velocity gradients, which in turn cause an increased turbulence production and hence also an increased mixing with the outer stream. This explains the observed reduction in wall temperature and hence in $\bar{\eta}$. This behaviour is different from that for the spacings s/D = 3 and 4.5 for which the individual jets penetrate into the boundary layer or even into the free-stream. For s/D = 1.5, the flow has wall-jet character anyway, so that good cooling effectiveness is achieved already and a faster bending-over of the jets does not necessarily increase the cooling effectiveness. This behaviour, which differs from that observed for the other situations, is reproduced correctly by the calculation procedure. Hence, it can be concluded, that overall the calculation procedure reproduces fairly well the observed film cooling behaviour and the influence of the density differences.

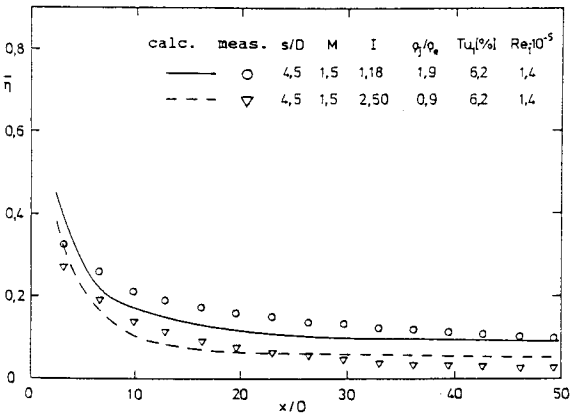


Fig.16: Cooling effectiveness on model turbine blade at s/D = 4.5, M = 1.5 and different density ratios; own measurements

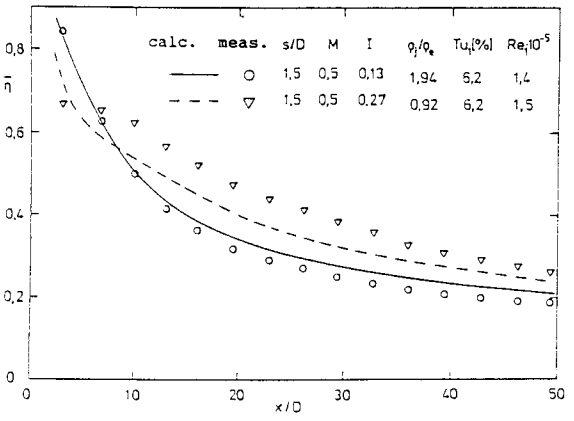


Fig. 17: Cooling effectiveness on model turbine blade at s/D = 1.5, M = 0.5 and different density ratios; own measurements

## 5. CONCLUSIONS

The film cooling model in the 2D boundary-layer procedure of Schönung and Rodi [1] was extended to account for the influence of density differences between hot gas and injected coolant gas. The model consists of two components, namely an injection model for setting up new boundary-layer profiles downstream of the immediate injection region and a dispersion model for simulating three-dimensional effects. In the course of introducing density effects with the aid of similarity considerations and experimental information, both models were reoptimised. The number of parameters for generating the new boundary-layer and the dispersion-term profiles could thereby be reduced. The extended model covers the full range of the parameters injection angle, relative spacing, blowing rate and density ratio of practical interest (see ranges given in Section 2.2). Also, the test calculations reported in [1] and here covered the following ranges of additional influence parameters: $0.05 \leq \delta^*/D \leq 0.25$, $1 \times 10^5 \leq Re_1 \leq 3 \times 10^5$, $10^3 \leq Re_j = U_j D/\nu \leq 4 \times 10^4$. The model was tested against flat-plate experiments and own experiments on a model turbine blade. The measurements have shown that the laterally averaged film cooling effectiveness increases with increasing density ratio $\rho_j/\rho_e$ at constant blowing rate. For the flat-plate cases, the predictions of the cooling effectiveness are in good agreement with the measurements except for small deviations near the injection. The film cooling effectiveness on the model blade is also generally predicted correctly. Only for configurations, for which surface-curvature effects not accounted for in the model play an important role, the agreement is not so good. However, in all cases the change in jet character due to the influence of density differences is simulated correctly. For constant density cases, the model was shown in [1, 2, 5] to predict satisfactorily also the heat transfer coefficient. As there are hardly any experimental studies on the influence of the density ratio on the heat transfer, the model was not tested for such situations. There is no reason to presume that it would not predict this influence satisfactorily too, but test calculations have yet to be carried out. Future research should also concentrate on the modelling of curvature effects and on the extension to film-cooling situations with injection from more than one row of holes.

## 6. ACKNOWLEDGEMENTS

The research reported here was sponsored partly by the Forschungsvereinigung Verbrennungskraftmaschinen e.V. The calculations were carried out on the Siemens 7881 computer of the University of Karlsruhe. The authors should like to thank Mrs. R. Zschernitz for preparing the typescript.

## 7. REFERENCES


[1] B. Schönung and W. Rodi: "Prediction of film cooling by a row of holes with a two-dimensional boundary-layer procedure". ASME Journal of Turbomachinery, Vol. 9, pp. 579-587, 1987.

[2] W. Haas, W. Rodi, B. Schönung: "Filmkühlung von Turbinenschaufeln durch Ausblasung aus einer Lochreihe". Zeitschrift für Flugwissenschaften und Weltraumforschung, 12, pp. 159-172, 1988.

[3] A.O. Demuren, W. Rodi, B. Schönung: "Systematic study of film cooling with a three-dimensional calculation procedure". Journal of Turbomachinery, Vol. 108, pp. 124-130, 1986.

[4] W. Haas, B. Schönung: "Erweiterte Version des Filmkühlmodells im Grenzschichtverfahren GRAFTUS/R zur Erfassung von Dichteunterschieden bei Filmkühlströmungen". Institut für Hydromechanik, Universität Karlsruhe, Bericht Nr. 662, Juni 1988.

[5] W. Haas: "Experimentelle und theoretische Untersuchungen zur Filmkühlung von Gasturbinenschaufeln". Dissertation, Universität Karlsruhe, 1989.

[6] H. Kruse: Messungen zur Filmkühlung". Deutsche Forschungs- und Versuchsanstalt für Luft- und Raumfahrt, Köln, Bericht Nr. 352-74/9, 1974.

[7] H. Kruse, H. Metzinger: "Der Einfluß der Belochungsgeometrie auf die Filmkühlwirkung einer Lochreihe". Deutsche Forschungs- und Versuchsanstalt für Luft- und Raumfahrt, Köln, Interner Bericht IB 325-9-84, 1984.

[8] C.J.P. Forth, P.J. Loftus, T.V. Jones: "The effect of density ratio on the film cooling of a flat plate". AGARD Conference Reprint No. 390, Heat Transfer and Cooling in Gas Turbines, Bergen, Norway, 6-10 May, 1985.

[9] D.R. Pedersen, E.R.G. Eckert, R.J. Goldstein: "Film cooling with large density differences between the main stream and secondary fluid measured by the heat mass transfer analogy". Journal of Heat Transfer, Vol. 99, pp. 620-627, 1977.

[10] N.W. Foster, D. Lampard: "The flow and film cooling effectiveness following injection through a row of holes". Journal of Engineering for Power, Vol. 102, pp. 584-588, 1980.

[11] S. Ito, R.J. Goldstein, E.R.G. Eckert: "Film cooling of a gas turbine blade". Journal of Engineering for Power, Vol. 100, p. 476, 1978.